Corrosion behaviour and mechanical properties of functionally gradient materials developed for possible hard-tissue applications

B. S. BECKER*, J. D. BOLTON
Engineering Materials Research Unit, Department of Manufacturing and Mechanical Engineering, University of Bradford, Richmond Road, Bradford, West Yorkshire BD7 1DP, UK

Artificial hip joints have an average lifetime of 10 years due to aseptic loosening of the femoral stem attributed to polymeric wear debris; however, there is a steadily increasing demand from younger osteoarthritis patients aged between 15 and 40 years for a longer lasting joint of 25 years or more. Compliant layers incorporated into the acetabular cup generate elastohydrodynamic lubrication conditions between the bearing surfaces, reduce joint friction coefficients and wear debris production and could increase the average life of total hip replacements, and other human load-bearing joint replacements, i.e. total knee replacements. Poor adhesion between a fully dense substrate and the compliant layer has so far prevented any further exploitation. This work investigated the possibility of producing porous metallic, functionally gradient type acetabular cups using powder metallurgy techniques – where a porous surface was supported by a denser core – into which the compliant layers could be incorporated. The corrosion behaviour and mechanical properties of three biomedically approved alloys containing two levels of total porosity ($>30\%$ and $<10\%$) were established, resulting in Ti–6Al–4V being identified as the most promising biocompatible functionally graded material, not only for this application but for other hard-tissue implants.

1. Introduction

Loosening of the femoral component of an artificial hip joint has been attributed to adverse tissue reactions against the ultra-high molecular weight polyethylene (UHMWPE) wear debris, causing bone necrosis around the implant. Recent attempts to minimize this risk have developed in four main directions: (1) the use of low elastic modulus implants [1–3], (2) improvements to the properties of bone cements [4–6], (3) biological fixation using porous implant coatings, and (4) the elimination of wear by using harder prostheses, either in the form of intrinsically hard materials (such as alumina ceramics [7, 8]), or by surface hardening (such as ion nitriding [9]).

None of these methods mimic the solution adopted by nature, i.e. the articular cartilage. Incorporating a compliant layer into the acetabular cup of an hip prosthesis would offer this alternative and has been shown to reduce friction levels to below 0.001, comparable with natural joints [10]; but integration of this compliant layer into a metallic substrate has proved problematic. Functionally gradient type materials, produced using conventional powder metallurgy techniques, offer the ideal solution, where the level of porosity can be graded, from a highly porous surface layer (suitable for polymer impregnation) to a dense core, giving the component suitable strength to withstand the physiological loadings. In the 1970s, this concept was used to produce femoral stems [11–13], but the work appeared to be abandoned due to concerns over poor fatigue performance, until a recent resurgence of interest [14, 15].

This work considers the corrosion behaviour and mechanical properties of three biomedically approved alloys, namely 316L stainless steel, a Co–29Cr–6Mo alloy and Ti–6Al–4V alloy, manufactured using the cold compaction and sintering route to contain two levels of total porosity ($>30\%$ and $<10\%$), with a view to producing a functionally graded acetabular cup suitable for polymer impregnation.

2. Materials and methods

Functionally graded specimens were obtained by sintering three alloys, namely water-atomized 316L, a novel bimodal Co–29Cr–6Mo powder mixture of water-atomized and ball-milled gas-atomized powder [16], and a Ti–6Al–4V alloy produced by blending

* Author to whom all correspondence should be addressed.
Selected paper from the 13th European Conference on Biomaterials, Göteborg, Sweden.

0957–4530

TABLE I Compositions (wt%) for the three metallurgical powders

Material	C	Cr	Ni	Mo	Si	Mn	Fe	Co	Al	V	Ti
316L	0.016	17.9	12.9	2.55	0.88	0.1	Bal.	–	–	–	–
Co–29Cr–6Mo	0.4	27.0	1.75	5.0	0.5	1.0	3.1	Bal.	–	–	–
Ti–6Al–4V	–	–	–	–	–	–	0.2	–	5.38	4.62	Bal.

TABLE II Summary of the powder processing variables altered to create a range of porous samples

Material property	316L stainless steel	Co–29Cr–6Mo alloy	Ti–6Al–4V alloy
Powder types	Water-atomized	Bimodal mix	Blended elemental
Powder particle sizes studied (μm)			
Coarse	152–104	–	353–250
Fine	<38	–	<63
Compaction pressure range (MPa)/intervals	308–926/154	470–1080/154	154–926/154
Sintering temperature range (°C)/intervals	1140–1315/95	1150–1350/100	1100–130/50 or 20

TABLE III Summary of green and sintered densities and total and interconnected porosities ranges created in each alloy

Material property	316L stainless steel	Co–29Cr–6Mo alloy	Ti–6Al–4V alloy
Green density range ($g\,cm^{-3}$)	5.0–6.8	5.0–6.5	2.65–4.0
Sintered density range ($g\,cm^{-3}$)	6.33–7.26	5.6–6.9 in vac. 5.6–7.5 in $Ar/H_2/N_2$[a]	3.24–4.31
Total porosity range (%)	35–9	33–17 in vac. 33–10 in Ar 32–6 in H_2/N_2[a]	30–3
Interconnected porosity range (%)	26–1	26–6 in vac. 26–0.5 in Ar 25–0.5 in H_2/N_2[a]	17–0.5

[a] Flowing molecular mixture (by volume) of 75%H_2/25% N_2.

titanium sponge with a 60V/40Al master alloy powder. Material compositions can be found in Table I.

2.1. Powder processing

Both the 316L stainless steel powder and the titanium sponge powder were sieved into seven different fractions, of which two were chosen for further study, a coarse and a fine fraction, (see Table II). Each powder was then compacted using a single-action manual press and sintered either under vacuum, or in a flowing molecular mixture of 75% H_2/25% N_2 (dewpoints better than $-55\,^{\circ}C$) or in flowing argon. Titanium alloys were only sintered under vacuum (better than 10^{-5} mbar). After sintering, densities, total porosities and interconnected porosities were measured using an adaptation of ASTM B328-73.

2.2. Corrosion testing

Potentiodynamic anodic polarization tests and open circuit potential–time transients were undertaken using a Sycopel Scientific Autostat 25V 1A computer-controlled potentiostat coupled to an Autoscan 16 channel multiplexer. Anodic polarizations tests were conducted in accordance with ASTM G5 except that the sweep rate was increased to $600\,mV\,min^{-1}$ to prevent sample destruction. A standard three-electrode cell was used with a saturated calomel reference electrode and graphite counter electrodes. In each test, the electrolyte was fully oxygenated Hank's solution (pH 7.4) maintained at $37\,^{\circ}C \pm 1\,^{\circ}C$. After corrosion testing, the electrolytes underwent trace element analysis by an inductively coupled plasma (ICP) method capable of detecting low metal ion concentrations.

Open circuit testing was undertaken for 24 h on the most porous alloys, using samples considered to have given the best potentiodynamic results.

2.3. Mechanical testing

Apparent hardness tests were carried out using a Vickers hardness testing machine with either a 10 or 20 kg load on the planar surfaces of samples polished to 1200 SiC grit. Young's modulus, ultimate tensile strength (UTS) and ductility were determined from tensile testing where $56 \times 14 \times 10$ mm blanks were machined to a gauge diameter of 6 mm over a length of 25 mm and tested on a computer-controlled Instron 5568. Initially, a 12.5 mm extensometer was used up to 0.1% strain, permitting Young's modulus to be determined, which was later verified by an ultrasonic method [15, 16]. The extensometer was then removed and the sample tested to fracture, enabling UTS and percentage elongation to be determined.

3. Results and discussion

Use of coarse and fine powders gave a range of total porosity from $\sim 5\%$ to $\sim 35\%$ with interconnected porosities of $\sim 0.5\%$ to $\sim 26\%$, as indicated in Table III. Different sintering mechanisms were observed

with each material and this affected the pore geometry and interconnected porosity, not only across the porosity range but also between materials.

316L sintered by solid-state diffusion in all atmospheres, therefore pore size and shape was largely dependent on compaction pressure and powder particle size and shape. Both Co–29Cr–6Mo and Ti–6Al–4V alloys appeared to consolidate through the formation of a transient liquid phase, at least at high sintering temperatures.

For the Co–29Cr–6Mo alloys this occurred due to localized melting around discrete carbides resulting in a eutectic liquid. The carbides consisted of either Cr_7C_3 or $Cr_{23}C_6$ and/or $Cr_2(C, N)$ depending on the sintering atmosphere.

Consolidation of Ti–6Al–4V powders appeared to be associated with the diffusion of aluminium away from the original master alloy, due to a reaction sintering mechanism rather than a transient liquid phase.

Changes to the sintering atmosphere varied the level of porosity in the bimodal Co–29Cr–6Mo alloys, especially when sintered above 1300 °C, with higher final densities being achieved in the H_2/N_2 gas mixtures than in the other atmospheres, as indicated in Table III.

Sintering atmospheres also had pronounced effects on microstructure in both 316L and Co–29Cr–6Mo alloys by causing severe chromium volatilization of the surface layers under vacuum, and reduction in carbide formation in the Co–29Cr–6Mo alloys. Sintering in molecular $75\%H_2/25\%N_2$ led to the cellular formation of chromium nitride (Cr_2N) lamellae in both alloys, whilst sintering in argon did not appear to alter the microstructure significantly.

3.1. Corrosion behaviour

Typical potentiodynamic anodic polarization behaviour for the three materials is shown in Fig. 1. From these curves a number of parameters were obtained, including the breakdown potentials, given in Fig. 2, i.e. where the transpassive region begins. This parameter was used as a performance indicator in this work, enabling the corrosion resistance for the three alloys to be ranked: 316L < Co–29Cr–6Mo < Ti–6Al–4V.

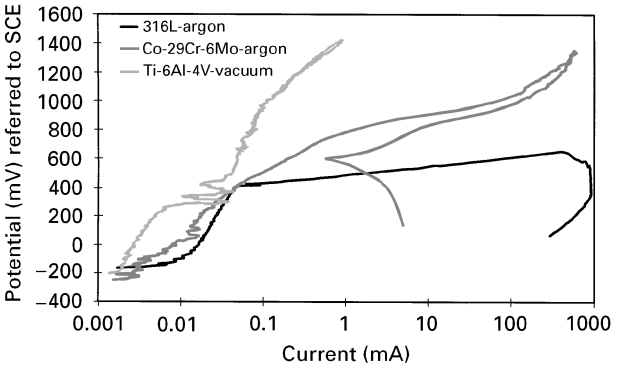

Figure 1 Typical potentiodynamic anodic polarization curves for 316L, Co–Cr–Mo alloy and Ti–6Al–4V alloy with a total porosity < 5% in oxygenated Hank's solution at a sweep rate of 600 mV min^{-1}. (Each curve is an average of three samples.)

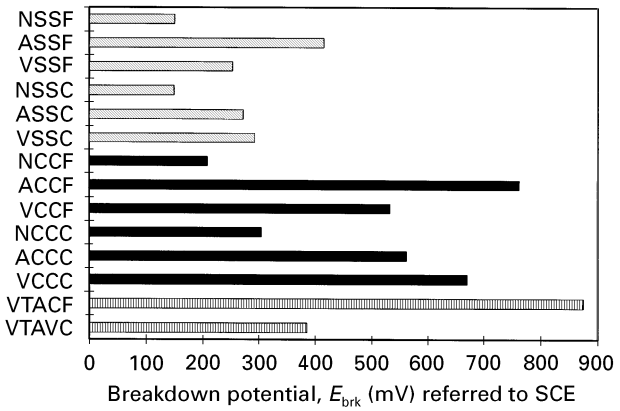

Figure 2 The effect of sintering atmosphere and porosity level on the breakdown potential in oxygenated Hank's solution after potentiodynamic anodic polarization testing. (N = molecular $75\%H_2/25\%N_2$, A = argon, V = vacuum, SS = stainless steel, CC = Co–29Cr–6Mo, TAV = Ti–6Al–4V, C = coarse total porosity (> 30%), F = fine total porosity (< 10%).)

Sintering atmosphere affected the corrosion behaviour of both the 316L and Co–29Cr–6Mo alloys; Cr_2N precipitates appeared locally to denude the matrix of chromium, leading to preferential attack at these sites. Loss in chromium at the surface after vacuum sintering, severely reduced corrosion resistance. The corrosion resistance of 316L and Co–29Cr–6Mo alloys was improved by sintering in argon. Overall, the effect of sintering atmosphere on corrosion performance was ranked H_2/N_2 < vacuum < argon.

Fig. 1 shows the size of the hysteresis loop obtained, which indicated the level of pitting attack that these samples experienced. As could be expected, 316L stainless steel exhibited the least resistance to pitting, while Ti–6Al–4V exhibited good resistance with no hysteresis. Scanning electron microscopy of the corroded surfaces indicated that severe pitting attack occurred with the stainless steels, intergranular attack and micro-pitting were evident with the bimodal Co–29Cr–6Mo but no obvious signs of corrosion were seen on the Ti–6Al–4V alloy.

Moreover, different levels of attack were seen in samples with different levels of porosity. Far greater attack was seen in the fine porosity samples compared to the coarse porosity samples, due to the fact that narrow pores helped to restrict ion diffusion/migration within the pore, so that concentration gradients were set up, such as the level of dissolved oxygen. Hydrolysis reactions leading to hydrogen-ion accumulation within the pore base, accelerated corrosive attack by reducing the pH. Oxygen depletion within the pore also helped to establish a more anodic region and further enhanced conditions which favoured crevice corrosion attack.

Trace ion levels were found to be considerably higher for 316L than Co–29Cr–6Mo alloys, as indicated in Fig. 3, indicative of faster corrosion rates for the 316L. There was also a noticeable difference in ion levels between the fine and coarse porosity samples for both alloys. This could not be attributed to differences in surface area, because the surface area of the fine porosity samples was lower than the coarse porosity

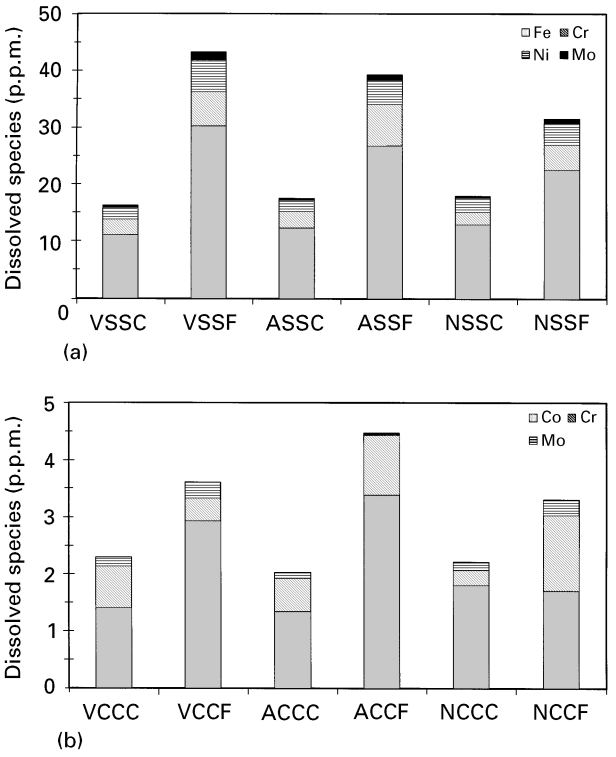

Figure 3 The effect of sintering atmosphere and porosity on ion release after anodic polarization testing in oxygenated Hank's solution. (a) Water-atomized 316L stainless steel, (b) bimodal Co–29Cr–6Mo alloys. (N = molecular 75%H_2/25%N_2, A = Argon, V = vacuum, SS = stainless steel, CC = Co–29Cr–6Mo, TAV = Ti–6Al–4V, C = coarse total porosity (> 30%), F = fine total porosity (< 10%).)

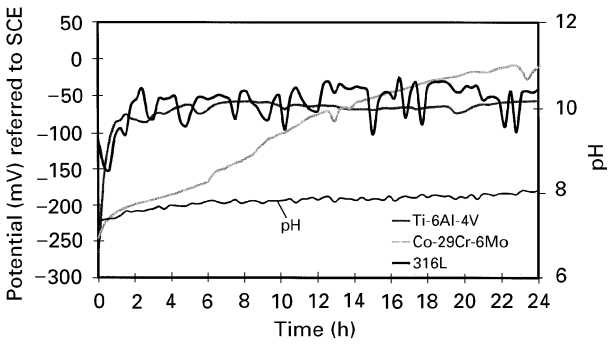

Figure 4 Potential–time transients over 24 h in oxygenated Hank's solution of coarse porosity samples with pH monitoring of the solution.

samples. Therefore, because of the presence of narrow pores in the fine porosity samples, faster corrosion rates must have occurred, resulting in greater dissolved ion levels.

Although Ti–6Al–4V alloys showed no signs of corrosive attack and no evidence of trace elements were found dissolved in solution, some low-level ion dissolution had taken place as corrosion currents were higher than for the wrought material. But this could have been due to surface-area effects caused by residual porosity.

Open circuit potential–time transients, in Fig. 4 gave an indication of the long-term behaviour of these materials. In the test, only argon-sintered 316L and Co–29Cr–6Mo alloys and a nitrided Ti–6Al–4V alloy

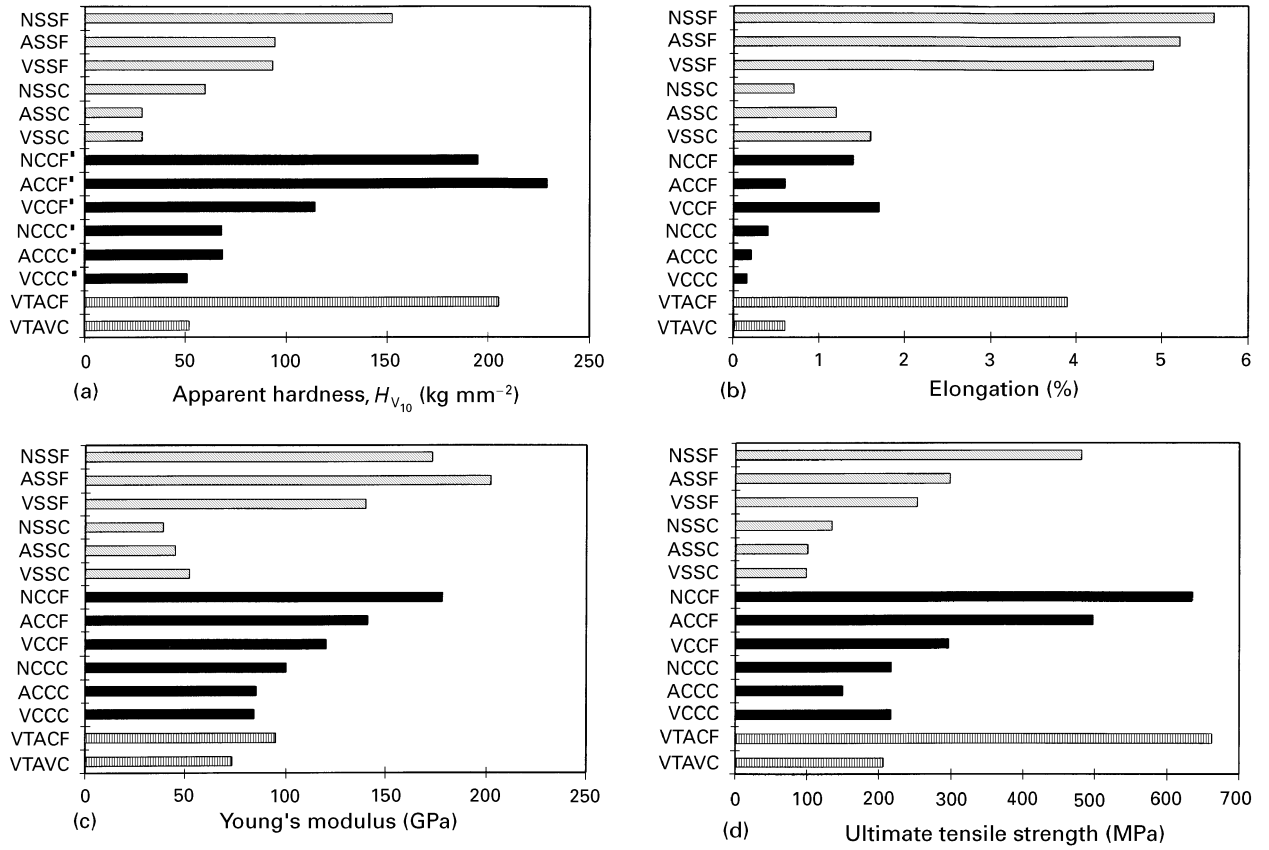

Figure 5 The effect of sintering atmosphere and porosity level on mechanical properties. (a) Apparent hardness, (b) percentage elongation, (c) Young's modulus, and (d) ultimate tensile strength. (N = molecular 75%H_2/25%N_2, A = Argon, V = vacuum, SS = stainless steel, CC = Co–29Cr–6Mo, TAV = Ti–6Al–4V, C = coarse total porosity (> 30%), F = fine total porosity (< 10%).)

were used. 316L underwent repeated film breakdown and repair associated with pitting attack, whilst both Co–29Cr–6Mo and Ti–6Al–4V alloys gave a rising transient which was indicative of the formation of a stable, protective, passive oxide film.

3.2. Mechanical properties

Increasing the level of porosity reduced the mechanical properties of these materials (see Fig. 5) especially hardness, tensile strength and percentage elongation. Variations in mechanical properties with sintering atmosphere were noted, particularly when Cr_2N precipitates had formed either in 316L or Co–29Cr–6Mo alloys; strengthening occurred, so that hardness and UTS values were consistently higher, but at the slight expense of ductility.

Fracture mainly occurred by ductile failure at interparticle necks and the size and number of these ductile failure sites increased in samples containing lower levels of interconnected porosities. Some brittle fractures were observed at the carbide/matrix interfaces in the Co–29Cr–6Mo alloy.

Although Co–29Cr–6Mo alloys had consistently higher hardness and UTS values, Ti–6Al–4V alloys combined high tensile strengths with larger amounts of plastic deformation taking place before final fracture. This was probably due to the pores acting as dislocation sinks, enabling substantial amounts of plastic deformation to be absorbed.

4. Conclusion

The corrosion resistance and mechanical properties of biocompatible materials containing two levels of porosity have been determined from which a functionally gradient type materials could be manufactured using the cold compaction and sintering route. Using titanium alloys combined the best biocompatibility with the best mechanical properties and therefore would be the most suitable porous materials for this application and could also find use as orthodontic or maxillofacial implants.

Acknowledgement

The work described was undertaken as part of BRITE/EuRam project, BE-4249-90. The authors would like to Dr Eric Jones, Howmedica International Inc., Limerick, Ireland, for providing the Co–Cr–Mo bar stock, and Dr Manuela M. Oliviera, Instituto Nacional Engenharia e Tecnologia Industrial (INETI), Lisbon, Portugal for undertaking the atomization of the Co–Cr–Mo alloy.

References

1. M. SEMLITSCH, H. WEBER and R. STEGER, in "Proceedings of the 8th World Conference on Titanium", edited by P. A. Blenkinsop, W. J. Evans and H. M. Flower (Institute of Materials, London, 1996) p. 1742.
2. T. AHMED, M. LONG, J. SILVESTRI, C. RUIZ and H. J. RACK, *ibid*., p. 1760.
3. Y. ITO, Y. OKAZAKI, A. ITO and T. TATEISHI, *ibid*., p. 1776.
4. Y. MIYAMOTO, K. ISHIKAWA, H. KUKAO, M. SWADA, M. NAGAYAMA, M. KON and K. ASAOKO, *Biomaterials* **16** (1995) 855.
5. S. DEB, M. BRADEN and W. BONFIELD, *ibid.* **16** (1995) 1095.
6. P. GRISS, G. V. HEIMKE and H. F. ANDRIAN-WERBERG, *Arch. Orthop. Infall-Chir.* **81** (1975) 259.
7. L. SEDEL, R. S. NIZARD, L. KERBOULL and J. WITVOET, *Clin. Othop. Rel. Res.* **298** (1994) 175.
8. P. KUMAR, M. OKA, K. IKEUCHI, K. SHIMIZU, T. YAMAMURO, H. OKUMURA and Y. KOTOURA, *J. Biomed. Mater. Res.* **25** (1991) 813.
9. R. A. BUCHANAN, I.-S. LEE and J. M. WILLIAMS, *ibid.* **24** (1990) 309.
10. A. UNSWORTH, *Proc. Inst. Mech. Eng. H* **205** (1991) 163.
11. J. S. HIRSCHHORN and J. T. REYNOLDS, in "Research in Dental and Medical Materials" edited by E. Korostaff (Plenum Press, New York, 1969) p. 137.
12. J. S. HIRSCHHORN, A. A. MCBEATH and M. R. DUSTOOR, in *J. Biomed. Mater. Res. Symp*., No. 2, Part 1 (1971) p. 49.
13. M. R. DUSTOOR and J. S. HIRSCHHORN, *Mod. Dev. Powd. Metall.* **11** (1979) 247.
14. H. HAHN, P. J. LARE, R. H. ROWE, A. C. FRAKER and F. ORDWAY JR., in "Corrosion and degradation of Implant Materials: Second Symposium", ASTM STP 859 edited by A. C. Fraker and C. D. Griffin (ASTM, Philadelphia, PA, 1985) p. 179.
15. B. S. BECKER and J. D. BOLTON, in "Proceedings of 1996 World Congress on Powder Metallurgy and Particulate Materials", edited by Terry M. Cadle and K. S. Narasimhan (MPIF, NJ, 1996) p. 14–119.
16. B. S. BECKER, J. D. BOLTON and M. YOUSEFFI, *Powd. Metall.* **38** (1995) 201.

Received 5 May
and accepted 12 May 1997